

OITS 762

March 2005

Parton and Hadron Correlations in Jets

Rudolph C. Hwa¹ and Zhiguang Tan^{1,2}

¹Institute of Theoretical Science and Department of Physics

University of Oregon, Eugene, OR 97403-5203, USA

²Institute of Particle Physics, Hua-Zhong Normal University, Wuhan 430079, P. R. China

Abstract

Correlation between shower partons is first studied in high p_T jets. Then in the framework of parton recombination the correlation between pions in heavy-ion collisions is investigated. Since thermal partons play very different roles in central and peripheral collisions, it is found that the correlation functions of the produced hadrons behave very differently at different centralities, especially at intermediate p_T . The correlation function that can best exhibit the distinctive features is suggested. There is not a great deal of overlap between what we can calculate and what has been measured. Nevertheless, some aspects of our results compare favorably with experimental data.

PACS numbers: 25.75.Gz, 25.75.Dw

1 Introduction

Correlations between hadrons produced in jets in heavy-ion collisions have become a subject of intense study recently [1]-[5]. There are many ways to describe the nature of the correlations, some using triggers, others giving correlations without triggers. So far no clear understanding of the properties of dihadron correlations has emerged. Satisfactory theoretical description of the problem is lagging even farther behind. In this paper we offer a theoretical view of some aspect of the correlations among partons and hadrons in connection with jets. Because we treat only a limited aspect of the dihadron distributions (notably only $\pi^+\pi^+$ correlation), we cannot make exhaustive comparisons with the data that have their own limitations, such as the lack of particle identification in many cases. Nevertheless, our results illuminate some important features of the nature of the correlations.

For experiments at the Relativistic Heavy Ion Collider (RHIC) the relevant range of transverse momenta (p_T) of the detected hadrons in which the correlations are probed is between 0.5 and 9 GeV/c. Since no calculation from first principles is reliable in the intermediate p_T range, any theoretical treatment of correlations can only be done in the framework of some phenomenological model. The parton recombination model has been successful in describing the single-particle inclusive distributions in Au+Au [6] as well as d+Au collisions [7, 8]. Indeed, it has already been applied to the study of some aspects of dihadron correlations [9]. We shall extend that study and examine in more detail various features of the correlations, not only among the produced hadrons, but also among the partons before they hadronize.

There are limitations to what we can do here. We shall continue to use the one-dimensional (1D) formulation of parton recombination, which offers a transparent display in

analytical forms the various components that contribute to dihadron correlations, without any thing hidden in an elaborate code. Focusing only on the p_T variable in the 1D treatment means that we cannot consider the dependencies on the pseudorapidity (η) and azimuthal angle (ϕ) separations between the two detected hadrons. That shortcoming will be overcome in a separate investigation. But by not being distracted by the behavior in $\Delta\eta$ and $\Delta\phi$ variables, we can examine more closely the separate roles that thermal and shower partons play in the correlation problem, when only the collinear momenta are considered. Experimentally, they correspond to the magnitudes of the associated particle momenta. Even with that simplification we have not considered all charged particles, which are what the experiments measure without particle identification. To gain an overview of the general properties of the correlation functions, the hadron pair $\pi^+\pi^+$ is sufficient and more transparent in providing a rich display of various features.

We shall first examine the single-particle distributions for Au+Au collisions at all centralities. The parameters determined can then be used for subsequent studies of correlations among partons and hadrons. The important ingredient in our investigation is the shower parton distribution functions, which were determined from the fragmentation functions [10]. In Sec. 3 the correlation among the shower partons is calculated both for jets in vacuum and for jets produced in heavy-ion collisions (HIC). They behave quite differently. Then we study in Sec. 4 the correlation among hadrons, for which the role of thermal partons becomes important in central collisions, but not as much in peripheral collisions. In Sec. 5 our results are compared with existing experimental data in areas where such comparisons are possible.

2 Single-Particle Distributions at all Centralities

In [6] the single-particle distribution of hadrons produced in Au+Au collisions at 200 GeV is studied for 0-10% centrality only. We now complete the picture by considering all other centralities, thereby determining the corresponding parameters for the thermal partons and the value of ξ that describes the average number of hard partons emerging from the dense medium to hadronize. This also gives us the opportunity to reiterate the basic equations for parton recombination.

The invariant inclusive distribution for a produced meson with momentum p is [6]

$$p \frac{dN_\pi}{dp} = \int \frac{dq_1}{q_1} \frac{dq_2}{q_2} F_{jj'}(q_1, q_2) R_\pi(q_1, q_2, p) \quad (1)$$

where the recombination function (RF) for a pion is [11]

$$R_\pi(q_1, q_2, p) = \frac{q_1 q_2}{p^2} \delta \left(\frac{q_1}{p} + \frac{q_2}{p} - 1 \right), \quad (2)$$

The distribution for two partons, j and j' , that are to recombine has three components

$$F_{jj'} = \mathcal{T}\mathcal{T} + \mathcal{T}\mathcal{S} + \mathcal{S}\mathcal{S}, \quad (3)$$

where the thermal parton distribution is

$$\mathcal{T}(q) = C q e^{-q/T}, \quad (4)$$

and the shower parton in $\mathcal{T}\mathcal{S}$ has the distribution

$$\mathcal{S}(q) = \xi \sum_i \int dk k f_i(k) S_i^j(q/k), \quad (5)$$

whereas the two shower partons in the same jet ($\mathcal{S}\mathcal{S}$) have the correlated distribution

$$(\mathcal{S}\mathcal{S})(q_1, q_2) = \xi \sum_i \int dk k f_i(k) \left\{ S_i^j \left(\frac{q_1}{k} \right), S_i^{j'} \left(\frac{q_2}{k - q_1} \right) \right\}, \quad (6)$$

$$\left\{ S_i^j(x_1), S_i^{j'}\left(\frac{x_2}{1-x_1}\right) \right\} = \frac{1}{2} \left[S_i^j(x_1) S_i^{j'}\left(\frac{x_2}{1-x_1}\right) + S_i^j\left(\frac{x_1}{1-x_2}\right) S_i^{j'}(x_2) \right]. \quad (7)$$

The distribution $f_i(k)$ of hard parton i at midrapidity in Au+Au collisions is given in [12].

The integral over k is from $k_{\min} = 3$ GeV/c to an upper limit which we shall set at 40 GeV/c.

S_i^j is a matrix of shower parton distributions (SPD) that have been determined in [10]. The form of the two SPDs, given in Eq. (7), symmetrizes the order of emission and guarantees the momentum conservation condition $x_1 + x_2 \leq 1$, apart from which the shower partons are assumed to be independent. Thus the correlation between the partons is essentially kinematical, as it is treated here, although other correlations of more dynamical origin can be considered later when the need arises.

The shower partons can either recombine among themselves, or recombine with the thermal partons. In the former case the process reproduces the fragmentation function

$$x D_i^\pi(x) = \int \frac{dx_1}{x_1} \frac{dx_2}{x_2} \left\{ S_i^j(x_1), S_i^{j'}\left(\frac{x_2}{1-x_1}\right) \right\} R_\pi(x_1, x_2, x). \quad (8)$$

Indeed, this is the equation from which the SPDs are determined in the first place [10]. Thus the \mathcal{SS} term in Eq. (3), when substituted into Eq. (1), yields the fragmentation component

$$p \frac{dN_\pi^{\mathcal{SS}}}{dp} = \xi \sum_i \int dk k f_i(k) \frac{p}{k} D_i^\pi\left(\frac{p}{k}\right), \quad (9)$$

Note that because the two shower partons are from the same jet, Eq. (9) depends linearly on $\xi f_i(k)$, which is the same dependence that the \mathcal{TS} component has. Hence, when all three terms in $F_{jj'}$ and the RF R_π are substituted into Eq. (1), we have, in the notation $p = p_T$,

$$\frac{dN_\pi}{dp} = \frac{C^2}{6} e^{-p/T} + \frac{\xi}{p} \sum_{ij} \int dk k f_i(k) \left[\frac{1}{k} D_i^\pi\left(\frac{p}{k}\right) + \frac{C}{p^2} \int dq_1 S_i^j\left(\frac{q_1}{k}\right) (p - q_1) e^{-(p-q_1)/T} \right]. \quad (10)$$

This is the basic formula for the inclusive distribution of pion. The hard parton i is summed over all relevant species, while j is summed over the two possible constituent quark species

of the pion. The quark j picks up a partner from the thermal environment to form the pion. That \mathcal{TS} component turns out to be dominant in the intermediate p_T region ($3 < p_T < 9$ GeV/c) in central Au+Au collisions, and is responsible for the high p/π ratio, when the production of proton is considered in a similar way [6].

We now apply Eq. (10) to non-central Au+Au collisions. The hard parton distribution $f_i(k)$ is scaled down from central collisions by the average number of binary collisions $\langle N_{\text{coll}} \rangle$. Our procedure is to fit the low- p_T data (for $p_T < 2$ GeV/c) by the first term that arises from \mathcal{TT} recombination, thereby determining C and T for each centrality. The only remaining parameter, ξ , is then determined by the overall normalization of the spectrum at each centrality so that the shape of the large p_T dependence is a prediction of Eq. (10). The data used are the π^0 spectra from PHENIX that extend up to $p_T = 10$ GeV/c [13]. We, however, calculate the π^+ distribution with $j = u$ and \bar{d} , since our formalism does not distinguish the two. Figure 1 shows the result of our calculation for four representative centralities, although we have treated all nine centralities, for which the parameters are shown in Fig. 2. Evidently, the spectra are well fitted at all centralities. The inverse slope T shows no significant dependence on centrality; the common value may be set at

$$T = 0.305 \text{ GeV/c.} \quad (11)$$

The value of ξ increases from 0.09 at 0-10% to 0.97 at 80-92% centrality. Thus Au+Au collision at 80-92% is essentially equivalent to pp collision, since the suppression factor due to energy loss is nearly 1, i.e., no jet quenching. The value of C decreases from 21.8 (GeV/c) $^{-1}$ at 0-10% to 2.3 (GeV/c) $^{-1}$ at 80-92%. The thermal component in peripheral collision is therefore much reduced, as expected.

The contributions from the various components are shown in Fig. 3 for 0-10% and 80-92% centralities. It is clear that at 0-10% the component from thermal-shower recombination is dominant in the $3 < p_T < 9$ GeV/c range, but at 80-92% that component is lower than both thermal-thermal and shower-shower components. Indeed, \mathcal{SS} dominates for all $p_T > 3$ GeV/c; it means that the fragmentation model is quite adequate for pp collisions in that p_T range.

3 Correlation of Partons in Jets

Before we consider the correlation between hadrons produced in jets, let us first study the simpler problem of correlation between partons in jets. Although the latter is not measurable, it provides a striking view of the difference between jets produced in vacuum, as in e^+e^- annihilation, and jets produced in HIC where the hard parton momentum is not fixed.

To define our notation, let $\rho_1(1)$ and $\rho_2(1, 2)$ be the single-particle and two-particle distributions, and we define the two-particle correlation function as

$$C_2(1, 2) = \rho_2(1, 2) - \rho_1(1)\rho_1(2) \quad . \quad (12)$$

Later, when we apply this formula to hadron correlation, the experimentally measurable quantities are

$$\rho_1(1) = \frac{dN_{\pi_1}}{p_1 dp_1}, \quad \rho_2(1, 2) = \frac{dN_{\pi_1 \pi_2}}{p_1 dp_1 p_2 dp_2}. \quad (13)$$

The normalized correlation function is

$$K_2(1, 2) = \frac{C_2(1, 2)}{\rho_1(1)\rho_1(2)} = r_2(1, 2) - 1 \quad , \quad (14)$$

where

$$r_2(1, 2) = \frac{\rho_2(1, 2)}{\rho_1(1)\rho_1(2)} \quad . \quad (15)$$

For reasons that will become evident below, it is useful to consider the ratio

$$G_2(1, 2) = \frac{C_2(1, 2)}{[\rho_1(1)\rho_1(2)]^{1/2}} \quad , \quad (16)$$

a quantity that is similar to the Pearson's correlation [14] under certain assumptions, and is closely related to a quantity considered in [2]

3.1 Two Shower Partons in a Jet in Vacuum

When a hard parton i with any fixed large momentum k fragments in vacuum to a shower of semi-hard and soft partons, we denote the single- and two-parton distributions in terms of the momentum fractions x_1 and x_2 by

$$\rho_1(1) = S_i^j(x_1) \quad , \quad (17)$$

$$\rho_2(1, 2) = (SS)_i^{jj'}(x_1, x_2) \quad , \quad (18)$$

where the RHS of Eq. (18) is to be identified with Eq. (7). For definiteness we consider $j = u$ and $j' = \bar{d}$. For $i = g$ we get for $r_2(1, 2)$ a 2D distribution as shown in Fig. 4. Other distributions with $i = u$ or \bar{d} are very similar.

Since $r_2(1, 2) = 1$ implies no correlation, we see from Fig. 4 that the two shower partons are uncorrelated when $x_1 \approx x_2 \approx 0$, but are highly correlated at higher x_i . Kinematical constraint due to momentum conservation forces $r_2(1, 2)$ to vanish at $x_1 + x_2 = 1$. It approaches zero faster, as $x_1 = x_2 \rightarrow 0.5$, than it does when x_2 is fixed and small, as

$x_1 \rightarrow 1 - x_2$. The implication is that if these two partons are to recombine to form a pion at $x = x_1 + x_2$, there is more contribution from the asymmetric pairing of x_1 and x_2 than from the unnecessarily stringent requirement that $x_1 = x_2 = x/2$.

3.2 Two Shower Partons in a Jet in HIC

For each event in HIC with a high p_T jet, we can calculate the two-parton distribution as above. However, the hard parton momentum k cannot be fixed in an experiment. The distribution in the shower parton momenta q_1 and q_2 , when averaged over all events, necessitates an integration over k and a sum over all i . The single-parton distribution

$$\rho_1(1) = \mathcal{S}^j(q_1) \quad (19)$$

is given by Eq. (5), while the two-parton distribution

$$\rho_2(1, 2) = (\mathcal{S}\mathcal{S})^{jj'}(q_1, q_2) \quad (20)$$

is given by Eqs. (6) and (7). Some details in the calculation need to be explained. When i in Eq. (6) is g , then $S_i^j S_i^{j'} = GG$, but when $i = u$, say, then $S_i^j S_i^{j'} = KL$, where G , K and L are SPDs initiated by gluon, valence quark and sea quark, respectively, in the notation of [10]. It turns out that the gross features of the results do not depend sensitively on these details.

For Au+Au collisions at 200 GeV we have calculated $r_2(1, 2)$. The results for most central and most peripheral collisions are shown in Fig. 5. The main feature is that $r_2(1, 2)$ is large and increases with q_1 and q_2 . That is markedly different from Fig. 4. The reason is that $\rho_1(1)\rho_1(2)$ depends quadratically on $\xi f_i(k)$, whereas $\rho_2(1, 2)$ depends on it linearly. The

probability $\xi f_i(k)$ for a hard parton to be produced at k in HIC is small in central collisions, and is even smaller in peripheral collisions (although ξ is larger) because $f_i(k)$ scales with $\langle N_{\text{coll}} \rangle$. Thus the probability of producing two partons in a jet is much higher than the product of the probabilities of producing the two partons separately. The latter does not require the two partons to be produced in two jets in the same event. For experiments at RHIC we may assume that events with two jets in the same hemisphere never occur, since they are so rare. Another way of interpreting $r_2(1, 2)$ is to write it as

$$r_2(1, 2) = \rho_c(2|1)/\rho_1(2) \quad , \quad (21)$$

where $\rho_c(2|1)$ is the conditional probability of finding a parton at q_2 given that a parton is at q_1

$$\rho_c(2|1) = \frac{\rho_2(1, 2)}{\rho_1(1)} \quad . \quad (22)$$

Thus $\rho_c(2|1)$ is like the distribution of a particle associated with a trigger at q_1 . The largeness of the ratio in Eq. (21) means that it is far more likely for a shower parton to be found at q_2 in association with another parton already found at q_1 than to find a parton at q_2 independently.

The two surfaces in Fig. 5 have essentially the same shape. The peripheral case is higher because the corresponding $\xi f_i(k)$ is smaller. In Fig. 4 the hard parton momentum k is held fixed and the probability of having such a parton is 1, while in Fig. 5 k is integrated up to 40 GeV/c so that at higher q_1 and q_2 there is no kinematical cut-off, albeit the probability $f_i(k)$ of producing a hard parton at higher k is greatly suppressed, which only makes $r_2(1, 2)$ higher.

The study in this section may seem academic, since shower partons are not directly observable. However, those shower partons are the main constituents that contribute to

the formation of pions that we shall treat in the following section. Their properties are therefore important to help us understand the features that we shall find about dihadron correlations. It should be emphasized that no free parameters have been used in this section, or in the section to follow, apart from C, T, ξ that have been determined in Sec. 2 for the single-particle distributions.

4 Correlation of Pions in Jets

For the production of two pions it is necessary to consider the recombination of four partons. The corresponding equation for the two-pion distribution is

$$\frac{dN_{\pi_1\pi_2}}{p_1 p_2 dp_1 dp_2} = \frac{1}{p_1^2 p_2^2} \int \left(\prod_{i=1}^4 \frac{dq_i}{q_i} \right) F_4(q_1, q_2, q_3, q_4) R_{\pi_1}(q_1, q_3, p_1) R_{\pi_2}(q_2, q_4, p_2). \quad (23)$$

The partons with momenta q_1 and q_3 that form π_1 can be either thermal or shower, as in Eq. (3). Similarly, the same is true with q_2 and q_4 . Thus F_4 has the form

$$F_4 = (\mathcal{T}\mathcal{T} + \mathcal{S}\mathcal{T} + \mathcal{S}\mathcal{S})_{13}(\mathcal{T}\mathcal{T} + \mathcal{S}\mathcal{T} + \mathcal{S}\mathcal{S})_{24} \quad . \quad (24)$$

Among the various possible combinations of terms, it is clear that $(\mathcal{T}\mathcal{T})_{13}(\mathcal{T}\mathcal{T})_{24}$ has nothing to do with hard scattering and contributes to the background. To subtract the background, one essentially considers the correlation function $C_2(1, 2)$. Despite the deceptive appearance of Eq. (24), F_4 is not factorizable. If it were, its substitution into Eq. (23) would render the factorizable form $\rho_2(1, 2) = \rho_1(1)\rho_2(2)$, implying no correlation. The nonfactorizability of F_4 is rooted in the correlations among the various shower partons. The correlation between two shower partons in $(\mathcal{S}\mathcal{S})_{13}$ or $(\mathcal{S}\mathcal{S})_{24}$ has already been considered in connection with Eq. (20), which is shown explicitly in Eqs. (6) and (7). However, those are not the correlations

that render F_4 nonfactorizable. It is the correlation between the partons in (1, 3) with the partons in (2, 4) that gives rise to nonvanishing $C_2(1, 2)$. More specifically, because all shower partons in Eq. (24) originate from the same hard parton at k , there is only one $\xi f_i(k)$ factor for all $\mathcal{SS} \cdots$ terms. Thus, for example, in $(\mathcal{ST})_{13}(\mathcal{ST})_{24}$ the $(\mathcal{SS})(q_1, q_2)$ term is exactly as expressed in Eq. (6). In $(\mathcal{ST})_{13}(\mathcal{SS})_{24}$ we can append $R_{\pi_2}(q_2, q_4, p_2)$ and make use of Eq. (8) to convert $(\mathcal{SS})_{24}R_{\pi_2}$ to D^{π_2} , so that the $(\mathcal{ST})(\mathcal{SS})$ contributions to $\rho_2(1, 2)$ is explicitly

$$\frac{dN_{\pi_1\pi_2}^{stss}}{p_1 p_2 dp_1 dp_2} = \frac{\xi}{p_1^3 p_2} \sum_{i,i',i''} \int dk k f_i(k) \int dq_1 \mathcal{T}(p_1 - q_1) \cdot \sum_j \frac{1}{2} \left[S_{i'}^j \left(\frac{q_1}{k} \right) \frac{1}{k - q_1} D_{i''}^{\pi_2} \left(\frac{p_2}{k - q_1} \right) + S_{i'}^j \left(\frac{q_1}{k - p_2} \right) \frac{1}{k} D_{i''}^{\pi_2} \left(\frac{p_2}{k} \right) \right] \quad (25)$$

which is not factorizable. For definiteness we shall hereafter consider π_1 and π_2 to be both π^+ . Then the sum in j is over u and \bar{d} . If $i = g$, then $i', i'' = g$; if $i = V$ (u or \bar{d}), then $(i', i'') = (V, S)$ or (S, V) where S denotes sea; if $i = S$, then $i', i'' = S$ also.

For completeness, let us write out the two other combinations of terms. For $(\mathcal{ST})_{13}(\mathcal{ST})_{24}$ we have

$$\frac{dN_{\pi_1\pi_2}^{stst}}{p_1 p_2 dp_1 dp_2} = \frac{\xi}{p_1^3 p_2^3} \sum_{i,i',i''} \int dk k f_i(k) \int dq_1 dq_2 \mathcal{T}(p_1 - q_1) \mathcal{T}(p_2 - q_2) \sum_{jj'} \left\{ S_{i'}^j \left(\frac{q_1}{k} \right), S_{i''}^{j'} \left(\frac{q_2}{k - q_1} \right) \right\} \quad , \quad (26)$$

where j and j' can be either u or \bar{d} . For $(\mathcal{SS})_{13}(\mathcal{SS})_{24}$ we have

$$\frac{dN_{\pi_1\pi_2}^{ssss}}{p_1 p_2 dp_1 dp_2} = \frac{\xi}{p_1 p_2} \sum_{i,i',i''} \int dk k f_i(k) \left\{ \frac{1}{k} D_{i'}^{\pi_1} \left(\frac{p_1}{k} \right), \frac{1}{k - p_1} D_{i''}^{\pi_2} \left(\frac{p_2}{k - p_1} \right) \right\} \quad . \quad (27)$$

In all three equations above i, i' and i'' follow the same rule stated at the end of the previous paragraph. For simplicity let us use the symbolic form for these three equations as follows: $[(\mathcal{ST})\mathcal{D}]$, $[(\mathcal{ST})(\mathcal{ST})]$ and $[\mathcal{D}\mathcal{D}]$, respectively. The parentheses imply the contents are to

recombine; the square brackets signify that the shower partons inside all arise from one hard-parton jet.

In $\rho_2(1, 2)$ the $(\mathcal{T}\mathcal{T})(\mathcal{T}\mathcal{T})$ term is factorizable, and is cancelled by the thermal terms in $\rho_1(1)\rho_1(2)$, where $\rho_1(1)$ is given by Eq. (10). That corresponds to background subtraction. Other double $\mathcal{T}\mathcal{T}$ terms like $(\mathcal{T}\mathcal{T})(\mathcal{S}\mathcal{T})$ also get cancelled. The surviving terms in $C_2(1, 2)$ all involve shower partons in each pion. We group them in four clusters of terms

$$C_2(1, 2) = C_2^{stst}(1, 2) + C_2^{stss}(1, 2) + C_2^{ssst}(1, 2) + C_2^{ssss}(1, 2) \quad , \quad (28)$$

where

$$C_2^{stst}(1, 2) = [(\mathcal{S}\mathcal{T})(\mathcal{S}\mathcal{T})]_{12} - (\mathcal{S}\mathcal{T})_1 * (\mathcal{S}\mathcal{T})_2 \quad (29)$$

$$C_2^{stss}(1, 2) = [(\mathcal{S}\mathcal{T})(\mathcal{D})]_{12} - (\mathcal{S}\mathcal{T})_1 * (\mathcal{D})_2 \quad (30)$$

$$C_2^{ssst}(1, 2) = [\mathcal{D}(\mathcal{S}\mathcal{T})]_{12} - (\mathcal{D})_1 * (\mathcal{S}\mathcal{T})_2 \quad (31)$$

$$C_2^{ssss}(1, 2) = [\mathcal{D}\mathcal{D}]_{12} - (\mathcal{D})_1 * (\mathcal{D})_2 \quad . \quad (32)$$

The products involving $*$ signify terms from $\rho_1(1)\rho_1(2)$, so their shower partons have their own hard partons. More precisely, $(\mathcal{S}\mathcal{T})_1 * (\mathcal{S}\mathcal{T})_2$, for example, has the explicit expression

$$\begin{aligned} (\mathcal{S}\mathcal{T})_1 * (\mathcal{S}\mathcal{T})_2 &= \left(\frac{\xi}{p_1^3} \sum_{ij} \int dk k f_i(k) \int dq_1 S_i^j \left(\frac{q_1}{k} \right) \mathcal{T}(p_1 - q_1) \right) \\ &\quad \cdot \left(\frac{\xi}{p_2^3} \sum_{ij} \int dk' k' f_i(k') \int dq_2 S_i^j \left(\frac{q_2}{k'} \right) \mathcal{T}(p_2 - q_2) \right) \quad . \end{aligned} \quad (33)$$

Clearly, this is very different from $[(\mathcal{S}\mathcal{T})(\mathcal{S}\mathcal{T})]_{12}$, written out in full in Eq. (26). Thus $C_2^{stst}(1, 2)$ does not vanish, in general, and likewise for the other terms in Eq. (28).

We have calculated all the quantities in Eqs. (28) - (32). The results cannot easily be displayed because each term decreases rapidly with p_1 and p_2 and the various clusters of terms, C_2^α , $\{\alpha = stst, \dots\}$, can be positive and negative, so that neither linear nor log plots are appropriate. To give a sense of the complication, we show in Fig. 6(a) the result for $\pi^+\pi^+$ correlation in central Au+Au collisions for the restricted case of $p_1 = p_2 = p$ in the range 1.5-10 GeV/c. At $p \approx 2$ GeV/c, all C_2^α become negative, resulting in a dip in C_2 . There is no such fine structure for peripheral collisions (80-92%), so a semi-log plot can exhibit the behaviors of C_2^α in the entire range up to $p = 10$ GeV/c, as shown in Fig. 6(b). Note that for 0-10% centrality the terms involving st component is dominant, while for 80-92% centrality the $\alpha = ssss$ component is dominant. These features are in accord with the properties of single-particle distributions shown in Fig. 3, where thermal-shower and shower-shower components, respectively, are dominant in the two cases.

When p_1 and p_2 are different, the two surfaces of $C_2(1, 2)$ for the two centralities are shown in Fig. 7 in the 2D ranges where they are positive. The region where $C_2(1, 2)$ is negative cannot be shown in the semi-log plot. For what can be shown they behave rather similarly. They both are suppressed by about 10 orders of magnitude going from 1 to 10 GeV/c. A large part of the rapid decrease is due to the power-law suppression that is present even in the single-particle distributions over the same p_T range, as can be seen in Fig. 1, though not more than 8 orders of magnitude. Thus the correlation function $C_2(1, 2)$ is not the best quantity to exhibit the properties of correlation.

To de-emphasize the power-law suppression of the hard parton distribution at high k that is contained in $\rho_1(1)$ and $\rho_1(2)$, we consider the normalized correlation $K_2(1, 2)$ defined in Eq. (14). When we set $p_1 = p_2 = p$, the dependence of $K_2(p)$ on p is shown in Fig. 8 for

(a) 0-10% and (b) 80-92% centrality. In (a) a dip occurs at low p , the minimum being at $p = 3$ GeV/c with $K_2 < 0$; in (b) there is no dip. The rapid rise at larger p is introduced into $K_2(1, 2)$ by the division of $C_2(1, 2)$ by $\rho_1(1)\rho_1(2)$, which is strongly damped at high p_1 and p_2 . It is the result of an over-correction. The fact that $K_2(80 - 92\%) \gg K_2(0 - 10\%)$ at all p in Fig. 8 is due to the property of $\xi f_i(k)$ being much smaller in peripheral collisions compared to central collisions. Since the numerator of $K_2(1, 2)$ depends linearly on $\xi f_i(k)$, but the denominator depends quadratically on it, the peripheral $K_2(1, 2)$ is therefore much larger.

What we see in Fig. 8 about the general features of $K_2(1, 2)$ for the two centralities is very similar to what is shown in Fig. 5 for $r_2(1, 2)$ for shower partons, recalling that $K_2(1, 2) = r_2(1, 2) - 1$, as stated in Eq. (14). Although $r_2(1, 2)$ cannot become negative, it becomes large in Fig. 5 at high q_1 and q_2 for both centralities. Of course, hadron correlation is far more complicated than parton correlation. But the common feature that they both become large at large parton and hadron momenta is due to the commonality in the definition of $r_2(1, 2)$ and $K_2(1, 2)$, which have $\rho_1(1)\rho_1(2)$ in the denominators.

It is now clear that we need something that is between $C_2(1, 2)$ and $K_2(1, 2)$ so as to have linear dependence on $\xi f_i(k)$ in both the numerator and the denominator. That quantity is the ratio $G_2(1, 2)$, defined in Eq. (16). Figure 9 shows the dependence of $G_2(1, 2)$ on $p_1 = p_2 = p$ for (a) 0-10% and (b) 80-92% centrality. Now, $G_2(p)$ is small at large p in both cases, and the properties of both can be revealed in linear plots. For 0-10% centrality there is still a dip at $p = 2$ GeV/c with $G_2(p) < 0$ in its vicinity, as it should, but for 80-92% centrality $G_2(p)$ decreases monotonically with increasing p . The normalizations of $G_2(p)$ for the two cases are now nearly the same. That can be seen more easily in semi-log plots. In Fig.

10 we show all three correlation function, C_2 , K_2 and G_2 , for the two centralities. The gap in Fig. 10(a) is due to the functions being negative in that range. Evidently, we have $C_2(0-10\%) \gg C_2(80-92\%)$, $K_2(0-10\%) \ll K_2(80-92\%)$, but $G_2(0-10\%) \approx G_2(80-92\%)$ in regions where they can be compared. Thus the function $G_2(1, 2)$ is best for the study of the nature of correlation.

In Fig. 11(a) we show $G_2(1, 2)$ in 2D distributions for both centralities in the same linear space. We now can see clearly their differences, knowing that asymptotically they behave similarly without structure. In the ranges of p_1 and p_2 plotted $G_2(1, 2)$ shows negative correlation for 0-10%, but positive correlations for 80-92% centrality. That difference can be succinctly exhibited in the ratio

$$R_{CP}^{G_2}(1, 2) = \frac{G_2^{(0-10\%)}(1, 2)}{G_2^{(80-92\%)}(1, 2)}, \quad (34)$$

which is shown in Fig. 11(b). Since peripheral Au+Au collisions at 80-92% centrality is very close to pp collisions, we may regard Fig. 11(b) as the clearest revelation of the difference in dihadron correlation between central Au+Au and pp collisions.

The origin of the hole in Fig. 11(b) can be found in Fig. 6 where C_2 is negative at $p_1 = p_2 = p = 2$ GeV/c for 0-10% centrality, but not for 80-92% centrality. The same is suggested by Fig. 7. The reason in physics involves the role that the thermal partons play in hadronization. In peripheral collision the shower-shower recombination component is dominant, as can be seen in Fig. 3(b). The thermal-thermal component is cancelled in $C_2(1, 2)$, so the shower-shower component, i.e. D in Eq. (8), dominates to very low p_T . For dihadron production double fragmentation, i.e. DD term in Eq. (27), is highly correlated, and is greater than $\mathcal{D} * \mathcal{D}$ in Eq. (32); hence $C_2^{ssss} > 0$. On the other hand, in central

collisions thermal-shower recombination is more important, as can be seen in Fig. 3(a) for $p_T < 8$ GeV/c. Again, $\mathcal{T}\mathcal{T}$ recombination can be ignored due to cancellation in $C_2(1, 2)$. Although the shower partons in a jet are correlated, the recombination of the shower partons with thermal partons results in weakened correlation between the pions formed, since the thermal partons are uncorrelated. Thus the $[(\mathcal{ST})(\mathcal{ST})]_{12}$ term in Eq. (29) can be weaker than the $(\mathcal{ST})_1 * (\mathcal{ST})_2$ term, even though the two shower partons in Eqs. (6) and (20) for the former term are correlated. That can happen only at low p_1 and p_2 , because at higher p_i the double power-law suppression of $(\mathcal{ST})_1 * (\mathcal{ST})_2$ provides no significant negative contribution to C_2^{stst} . For these reasons we get a hole in $R_{CP}^{G_2}(1, 2)$.

5 Comparison with Experimental Data

In the foregoing we have studied the correlation of two π^+ without using any adjustable parameters. What we have obtained unfortunately cannot be compared directly with current data, because most experiments either do not yet have particle identification, or put emphasis on jets with trigger particles and study the dependencies on $\Delta\phi$ and $\Delta\eta$ of associated particles. There are, however, two areas in which our theoretical calculations come close to the experimental data and are of interest for us to examine them in more detail here.

The first area concerns the experiment in [5], in which data are given for the p_T distribution of charged particles associated with trigger in the range $4 < p_T < 6$ GeV/c. We can come close to what is measured by calculating

$$\frac{dN_{\pi^+}^{tr-bg}}{p_2 dp_2} = \int_4^6 dp_1 p_1 \frac{dN_{\pi^+\pi^+}^{tr-bg}}{p_1 p_2 dp_1 dp_2} / \int_4^6 dp_1 p_1 \frac{dN_{\pi^+}}{p_1 dp_1}, \quad (35)$$

where p_1 is regarded as the momentum of the trigger particle, and p_2 that of the associated

particle. The superscript, $tr - bg$, denotes the sample of triggered events with background subtracted. For the integrand in the numerator we use Eq. (23), but with F_4 not given by Eq. (24). Background subtraction corresponds in our case to leaving out in Eq. (24) the terms that are factorizable. We are uncertain whether that correspondence is exact, since the experimental procedure for the determination of the background is not unique and involves steps that seem hard to duplicate in theoretical calculation. Our procedure of retaining only the non-factorizable component is the most sensible way to obtain the associated particle distribution, so we use

$$F_4^{tr-bg} = (\mathcal{ST} + \mathcal{SS})_{13}(\mathcal{ST} + \mathcal{SS})_{24}, \quad (36)$$

which is not factorizable because of the correlation that exists between the shower parton at q_1 and the shower parton at q_2 , as we have studied in Sec. 3.

We note that Eq. (35) is a ratio of the integrals over the trigger momentum in contrast to the integral of the ratio that is calculated in [9]. Eq. (35) corresponds to the way that the data are presented in [5].

There is one piece of detail about the calculation using Eqs. (23) and (36) that we now discuss. Among the SPDs determined in [10] the gluon initiated quark distribution has a parametrization that leads to divergence, $G(x) \propto x^{-a}$, as the momentum fraction $x \rightarrow 0$. It is unphysical in that limit, although the parametrization renders a good fit of the fragmentation function away from that limit. In application to the calculation of dN_π/pdp , as in Eq. (10), the integral over q_1 is convergent, and at small p the \mathcal{ST} component is dominated by the \mathcal{TT} component. But when the background is subtracted with the $(\mathcal{TT})(\mathcal{TT})$ component removed from $dN_{\pi\pi}/p_1 p_2 dp_1 dp_2$, the effect of large $G(x)$ at very small x is exposed. Since

that effect is unphysical and since we do not claim reliability of our formalism at very small p_T , we introduce an *ad hoc* factor

$$s(q) = 1 - e^{-q} \quad (37)$$

to suppress the distribution at small q for all gluon initiated shower partons. This procedure does not affect the results of our calculation for $p_T > 1.5$ GeV/c, but does introduce a round-off at lower p_T in the associated particle distribution. Figures in Sec. 4 all have that factor $s(q)$ included for gluon initiated showers.

Substituting Eq. (36) into Eq. (23) and then into Eq. (35), we obtain the results shown in Fig. 12 for (a) 0-10% and (b) 80-92% centralities. The calculated curves are for π^+ trigger and π^+ associated particle, while the data points from [5] are for all charged particles with 0-5% centrality in (a) and for pp collision in (b). The shapes of the p_T dependence agree very well; the normalizations differ by a factor that can be attributed to the data being for all charged particles. Thus our formalism describes the correlation between particles in jets quite satisfactorily when compared to data.

Another area of possible comparison between theory and experiment is in correlation at low p_T . Data on a quantity denoted by $\Delta\rho/\sqrt{\rho}$ in Ref. [2] for pp collision show a bulge plotted in transverse rapidity, defined by

$$y_t = \ln[(m_T + p_T)/m_\pi]. \quad (38)$$

Since the quantity $\Delta\rho/\sqrt{\rho}$ is rather similar to our $G_2(1, 2)$, it is of interest to display the latter in terms of y_t , which has the virtue of expanding the low p_T scale. Figure 13 shows y_t as a function of p_T . Since our calculations are unreliable for $p_T < 1$ GeV/c, we consider

only the region $y_t > 2.5$. Instead of Eq. (13), we now define

$$\rho_1(1) = \frac{dN_{\pi_1}}{dy_1}, \quad \rho_2(1, 2) = \frac{dN_{\pi_1\pi_2}}{dy_1 dy_2}, \quad (39)$$

where $dy_i = dp_i/m_T$. $C_2(1, 2)$ and $G_2(1, 2)$ remain to be defined by Eqs. (12) and (16), respectively, but in terms of y_1 and y_2 they are changed in accordance to Eq. (39).

In Fig. 14 we show $G_2(1, 2)$ as functions of y_1 and y_2 for (a) 80-92% and (b) 0-10% centralities. They are reproductions of the two surfaces in Fig. 11(a), now in terms of y_i . The upper ones in both are for peripheral collisions, while the lower ones are for central collisions. The increase at small y_1 and y_2 in Fig. 14(a) appears to agree with the bulge in the pp collision data in [2] for $y_1, y_2 > 2.5$. For central collision Fig. 14(b) has a peak and a dip, which are predictions that should be checked by the analysis of the corresponding data. For completeness, we show in Fig. 15 the $R_{CP}^{G_2}$ in the y_1, y_2 variables, in terms of which the dip becomes the dominant feature, even more prominent than in Fig. 11 (b).

6 Conclusion

We have calculated the single-particle distribution in Au+Au collisions at all centralities, and considered various types of correlation functions in jets. For correlations between shower partons we have shown the drastic difference between the case when the hard parton momentum k is fixed, as in e^+e^- annihilation, and the case in heavy-ion collisions where k is not fixed. For hadron correlations we have considered three types of correlation functions, $C_2(1, 2)$, $K_2(1, 2)$, and $G_2(1, 2)$, and showed that $G_2(1, 2)$ is best in displaying the structure of the dihadron correlation.

We have found that the ratio of $G_2(1, 2)$ for central collisions to that for peripheral collisions has a big dip in the $p_1 \approx p_2 \approx 2$ GeV/c region. That is where the correlation between shower partons in a jet is diluted by their recombination independently with thermal partons in central Au+Au collisions. However, in peripheral collisions there is no abundance of thermal partons in the shower environment, so the shower partons recombine with themselves, resulting in strong correlation. The calculated features of $G_2(1, 2)$ can be checked by experiment, since all the quantities involved are directly measurable.

Although most of the results obtained on the correlation functions cannot be compared with any existing data, there is no basic hurdle to overcome for the data analysis to be carried out in ways that can check our prediction. The distribution of associated particles that we have calculated for $\pi^+\pi^+$ correlation compares satisfactorily with the data except for the normalization difference due to the fact that the data are for all charged particles. Our result on G_2 for peripheral collisions has some resemblance to the data on pp collisions, which are, however, not presented in a way that can facilitate quantitative comparison. Clearly, closer coordination between theoretical and experimental efforts would be of great value to both.

In this work the basic quantity is the correlation function $C_2(1, 2)$ that is precisely defined. By subtracting $\rho_1(1)\rho_1(2)$ from $\rho_2(1, 2)$, not only is the background subtracted, other factorizable terms are taken out too, creating the possibility that $C_2(1, 2)$ can become negative. That possibility does not show up in the present experimental way of determining the associated particle distribution [3, 5], but may be present in other ways of studying correlations [1, 2, 4]. We suggest that future experimental work be directed toward determining the correlation function $G_2(1, 2)$ and the central-to-peripheral ratio $R_{CP}^{G_2}(1, 2)$. The

absence of any hole in the experimental result on $R_{CP}^{G_2}(1,2)$, as shown in Figs. 11(b) and 15, would provide valuable information on the nature of parton correlation that we have not incorporated in our formulation of the problem.

Acknowledgment

We are grateful to Tom Trainor and Fuqiang Wang for valuable communication on their work and to C. B. Yang for helpful comments. This work was supported, in part, by the U. S. Department of Energy under Grant No. DE-FG03-96ER40972.

References

- [1] T. A. Trainor (STAR Collaboration), talk given at the 20th Winter Workshop on Nuclear Dynamics, Jamaica, 2004, hep-ph/0406116.
- [2] R. J. Porter and T. A. Trainor, *Acta Physica Polonica B* **36**, 353 (2005).
- [3] D. Magestro, Proceedings of Hard Probes 04, Ericeira, Portugal (2004).
- [4] J. Adams et. al., (STAR Collaboration), nucl-ex/0406035, 0408012, 0411003.
- [5] J. Adams et. al., (STAR Collaboration), nucl-ex/0501016.
- [6] R. C. Hwa and C. B. Yang, *Phys. Rev. C* **70**, 024905 (04).
- [7] R. C. Hwa and C. B. Yang, *Phys. Rev. Lett.* **93**, 082302 (04); *Phys. Rev. C* **70**, 037901 (04).

- [8] R. C. Hwa, C. B. Yang and R. J. Fries, Phys. Rev. C **71**, 024902 (2005).
- [9] R. C. Hwa and C. B. Yang, Phys. Rev. C **70**, 054902 (2004).
- [10] R. C. Hwa and C. B. Yang, Phys. Rev. C **70**, 024904 (2004).
- [11] R. C. Hwa and C. B. Yang, Phys. Rev. C **66**, 025205 (2002).
- [12] D. K. Srivastava, C. Gale, and R. J. Fries, Phys. Rev. C **67**, 034903 (2003).
- [13] S. S. Adler *et al* (PHENIX Collaboration), Phys. Rev. Lett. **91**, 072301 (2003).
- [14] E. W. Weinsstein, *Correlation Coefficient*, MathWorld – A Wolfram Web Resource.
<http://mathworld.wolfram.com/CorrelationCoefficient.html>.

Figure Captions

Fig. 1. Single-particle distributions of produced π in Au+Au collisions at $\sqrt{s} = 200$ GeV for four centrality cuts. Data are from [13], and the solid lines are the results of calculation in the recombination model.

Fig. 2. The three parameters C, T and ξ , determined by fitting the data at all centralities.

Fig. 3. The single-particle distributions for (a) most central and (b) most peripheral collisions, showing the three components that contribute to the sums in solid lines.

Fig. 4. The ratio $r_2(1, 2)$ in terms of the shower parton momentum fractions x_1 and x_2 for a hard gluon momentum fixed at a large values k .

Fig. 5. The ratio $r_2(1, 2)$ in terms of the shower parton momenta q_1 and q_2 in heavy-ion collisions for two extreme centralities.

Fig. 6. The correlation functions C_2 for $\pi^+\pi^+$ in HIC, showing the contributions from the three combinations of \mathcal{S} and \mathcal{T} partons for (a) central and (b) peripheral collisions along the diagonal where $p_1 = p_2$.

Fig. 7. The correlation functions C_2 for two centralities when they are positive.

Fig. 8. The normalized correlation functions K_2 along the diagonal where $p_1 = p_2$ for (a) central and (b) peripheral collisions.

Fig. 9. The partially normalized correlation functions G_2 along the diagonal where $p_1 = p_2$ for (a) central and (b) peripheral collisions.

Fig. 10. A comparison of the three types of correlation functions C_2 , K_2 and G_2 in semi-log plots, with the gap corresponding to where the functions are negative.

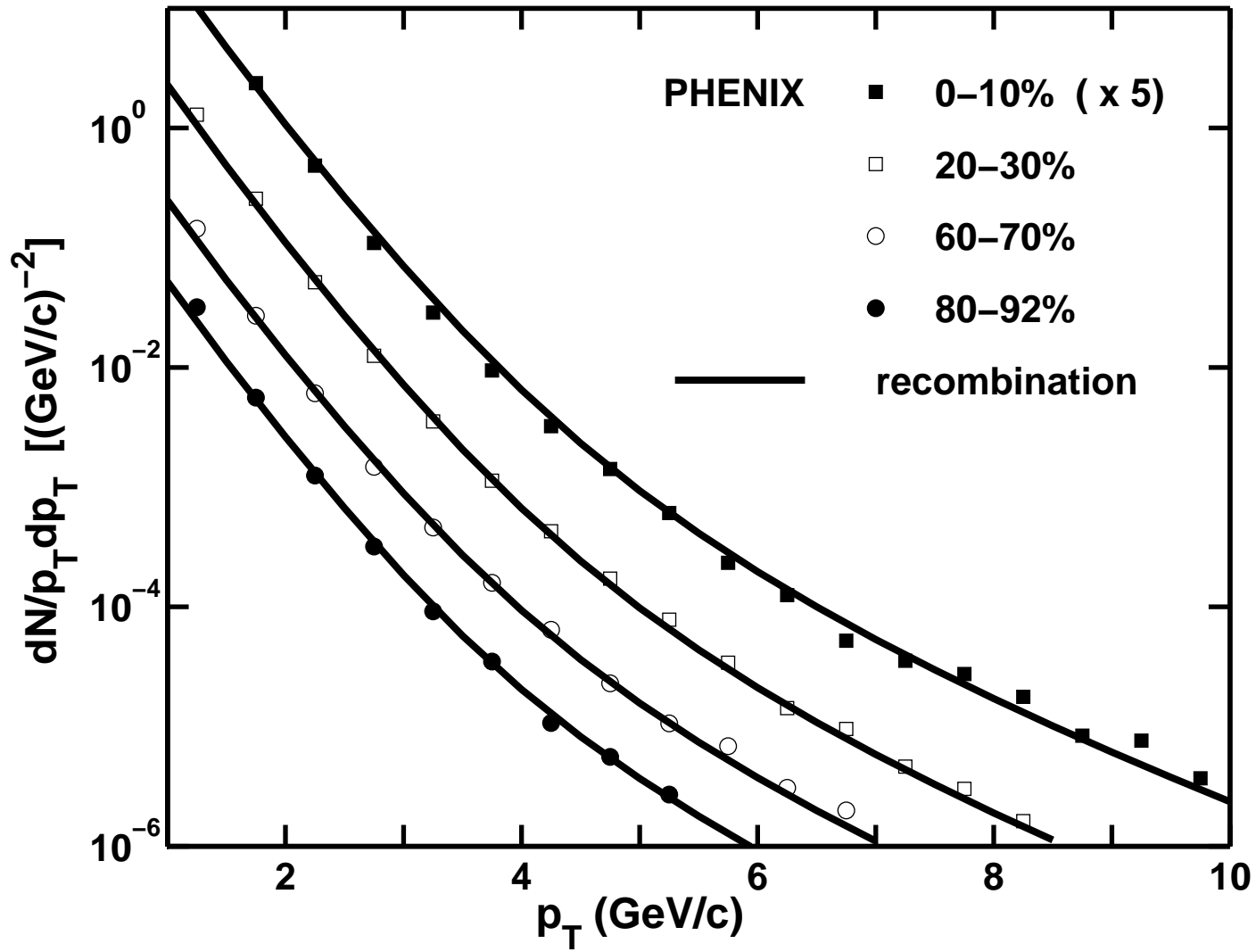
Fig. 11. (a) $G_2(1, 2)$ plotted as functions of p_1 and p_2 for two centralities; (b) the ratio $R_{CP}^{G_2}$ of central to peripheral G_2 .

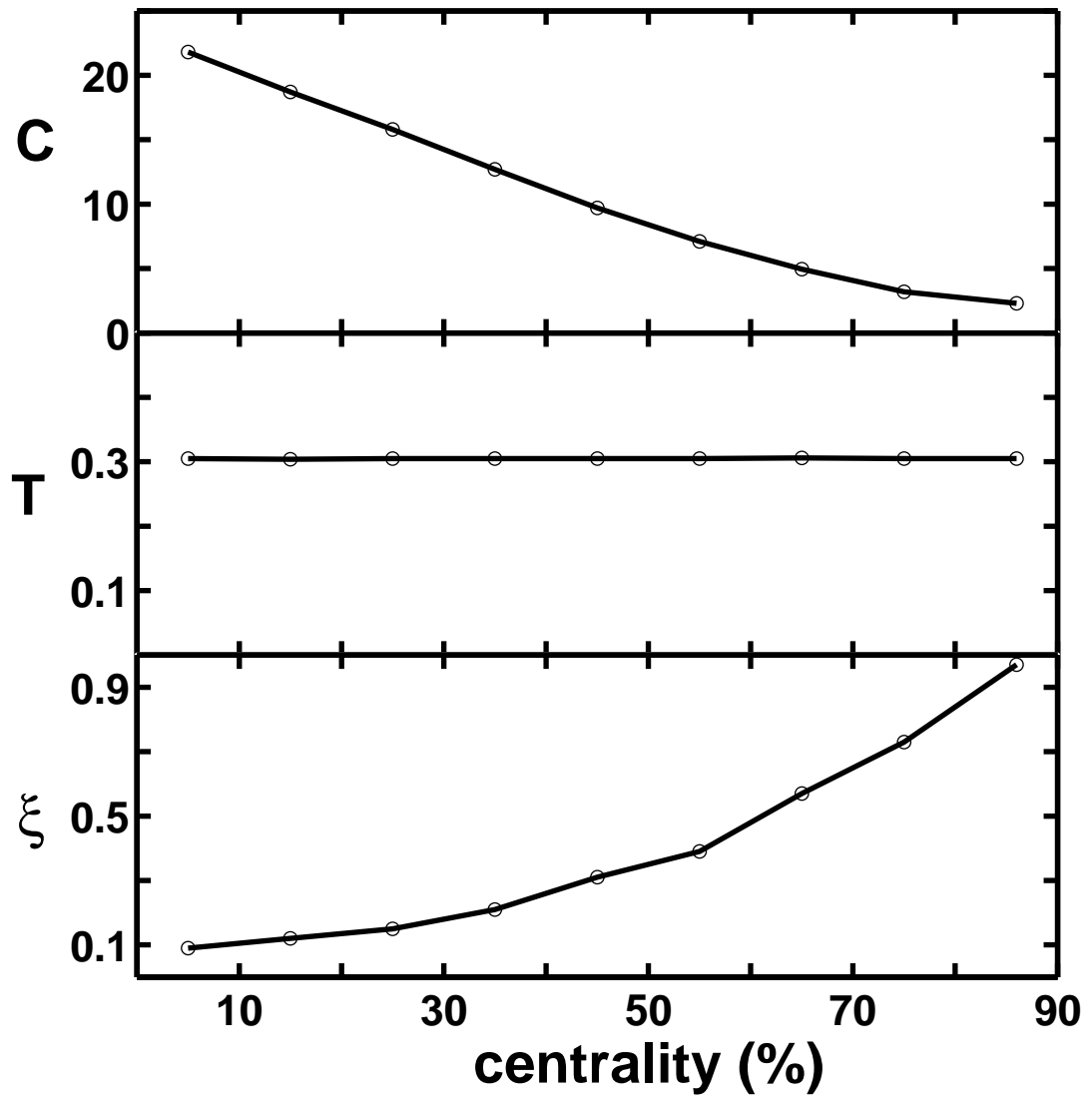
Fig. 12. Associated particle distributions of $\pi^+\pi^+$ for (a) central (0-10%) collisions compared to the STAR data [5] for all charged particles at (0-5%) centrality and (b) peripheral (80-92%) collisions compared to the STAR data [5] for all charged particles in pp collisions.

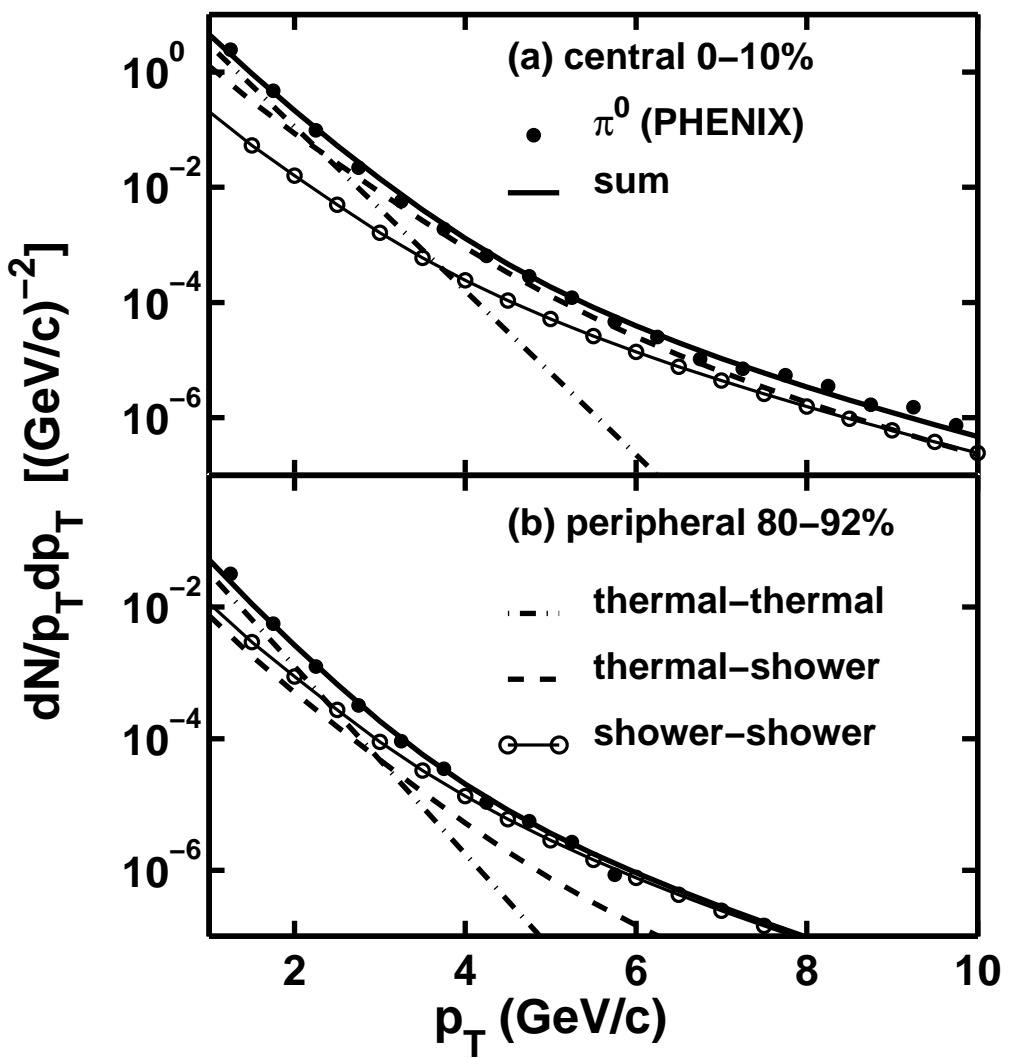
Fig. 13. Transverse rapidity as a function of p_T .

Fig. 14. $G_2(1, 2)$ for $\pi^+\pi^+$ plotted in terms of transverse rapidities for (a) peripheral (80-92%) and (b) central (0-10%) collisions.

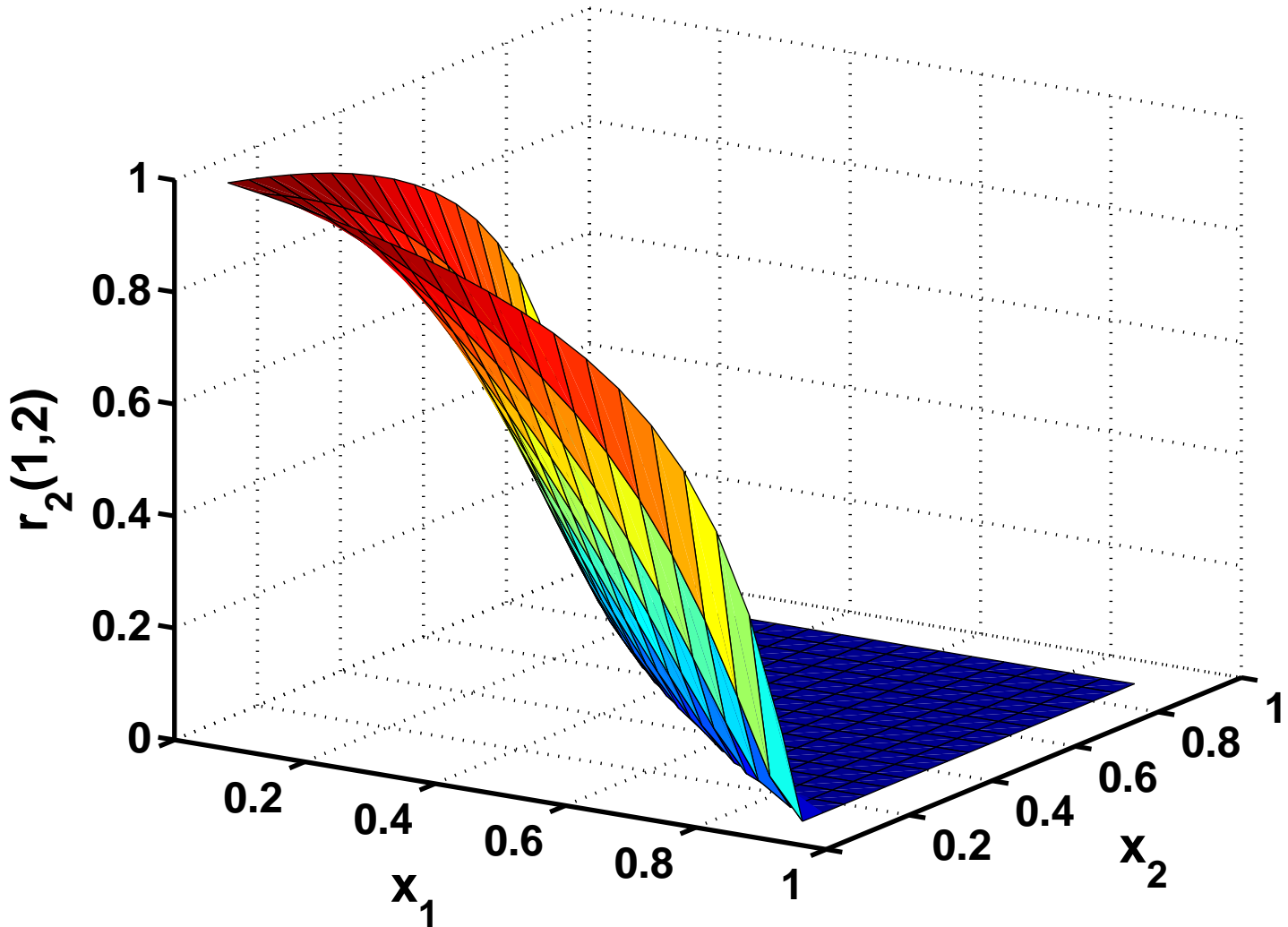
Fig. 15. The ratio $R_{CP}^{G_2}$ in transverse rapidities.







Shower partons with fixed k



Shower partons in HIC

